

CERN-TH/2003-282

Cross sections for multi-particle final states at a linear collider

T. Gleisberg^{1 a}, F. Krauss^{1,2 b}, C. G. Papadopoulos^{2,3 c}, A. Schälicke^{1 d}, and S. Schumann^{1 e}¹ Institut für Theoretische Physik, TU Dresden, 01062 Dresden, Germany² Theory Division, CERN, 1211 Geneva 23, Switzerland³ Institute of Nuclear Physics, NCSR Demokritos, 15310 Athens, GreeceNovember 21st 2003

Abstract. In this paper total cross sections for signals and backgrounds of top- and Higgs-production channels in e^+e^- collisions at a future linear collider are presented. All channels considered are characterized by the emergence of six-particle final states. The calculation takes into account the full set of tree-level amplitudes in each process. Two multi-purpose parton level generators, HELAC/PHEGAS [1,2] and AMEGIC++ [3] are used, their results are found to be in perfect agreement.

1 Introduction

Six-particle final states constitute the signature for many processes that will be studied at the precision level at a future e^+e^- linear collider. Important channels include the production and decay of top quark pairs and – if existent – of one or more Higgs bosons, the latter process allowing a test of the structure of the Higgs potential. Furthermore, if no evidence for a Higgs boson was found at the LHC, the study of quartic gauge boson couplings is mandatory in order to understand alternative scenarios of electroweak symmetry breaking. Leaving the framework of the Standard Model (SM) the production of, say, chargino pairs in the Minimal Supersymmetric Standard Model (MSSM) will lead to six-particle final states as well. To understand these processes at the precision level, i.e. at the order of a few per cent, it is mandatory to supplement typical approaches such as the narrow-width approximation, with corresponding calculations through full amplitudes, and to quantify the effect of non-resonant contributions. Obviously, for hadronic final states, a full QCD calculation is unavoidable.

Such investigations, however, are a formidable calculational task that cannot be handled without dedicated computer programs. Two major difficulties make these necessary:

1. Including the full SM for the production of a six-particle final state often leads to having to handle a large number of diagrams. As an illustrative example of this

problem, take the process $e^+e^- \rightarrow e^+e^-e^+e^-e^+e^-$, which results in 13896 Feynman diagrams. Obviously, the common textbook method of squaring the diagrams, by employing completeness relations for the external particles and evaluating the traces, is not a very efficient way to calculate the matrix element squared.

2. Apart from the treatment of an enormous number of diagrams, growing roughly factorially with the number of external legs, the integration over the phase space of the outgoing particles becomes a tedious task. The high dimensionality, $3n - 4$, for n final-state particles necessitates the use of Monte Carlo methods. To achieve convergence of the Monte Carlo procedure process- and cut-dependent phase-space mappings are required that tame wildly fluctuating integrands, which are due to nearly on-shell propagators. A benefit of Monte Carlo methods, if carefully implemented, is that not only total cross sections but also distributions including all possible types of kinematical cuts can be calculated on an equal footing.

In the past years, different types of parton level generators have been constructed. They can be crudely characterized as either specialized or multi-purpose generators.

Usually, the former ones contain explicit matrix elements and phase-space mappings for specific classes of processes with specific assumptions. These matrix elements were constructed before outside the respective program, and this feature also allows for instance to implement non-universal higher order corrections in a controlled way. Often, the phase space mappings can be optimized before as well.

Examples for such programs dealing with some of the processes discussed here are LUSIFER [4] and eett6f [5]. Both are constrained to fermions in the final state; in the case of

^a email: tanju@theory.phy.tu-dresden.de^b email: Frank.Krauss@cern.ch^c email: Costas.Papadopoulos@cern.ch^d email: dreas@theory.phy.tu-dresden.de^e email: steffen@theory.phy.tu-dresden.de

LUSIFER these fermions are bound to be massless, whereas **eett6f** specializes in top quark pair production channels where the outgoing fermions might be massive, but electrons are disallowed in the final state. Both programs use versions of the adaptive multichannel method in the spirit of [6] for their integration. A further dedicated program using the multichannel importance sampling is **SIXFAP** [7]. It provides the electroweak contributions for a large set of six-fermion final states, taking into account possible non-zero fermion masses.

In contrast to specialized programs, multipurpose codes generate both the matrix elements and the phase space mappings with or without some intervention by the user. Apart from the programs used in this paper, examples of these types of programs are **O'Mega/Whizard** [8,9] and **MadGraph/MadEvent** [10,11]. In the first package, **O'Mega** [8] relies on a version of the **alpha** algorithm [12]. However, in the present version of **O'Mega**, full QCD has not been implemented yet. The integration of the resulting matrix elements is achieved through **Whizard** [9], which constructs phase-space mappings automatically and integrates them with the **VAMP**-algorithm [13]. In fact, **Whizard** can also be interfaced with other matrix element generators and it can be used to generate unweighted, single events. In contrast, **MadGraph/MadEvent** generates all Feynman diagrams for a process under consideration and then passes the information to the **HELAS** package [14] for the translation into corresponding helicity amplitudes. The integration channels are constructed automatically, and a new version of the adaptive multichannel method described in [11] is employed for the actual integration and the generation of unweighted events.

This paper deals with the calculation of total cross sections for many relevant processes at a future e^+e^- collider with two different, independent packages, namely **HELAC/PHEGAS** and **AMEGIC++**. Similar to the comparison of four-fermion generators at the LEP2 Monte Carlo Workshop [15], a detailed study and mutual benchmarking of tools for six- and eight-particle final states at a future linear collider has been initiated in the framework of the extended ECFA/DESY study [16]. Here, a further step into this direction is reported.

For the case of only massless final state particles, a similar comparison between the programs **LUSIFER** and **MADGRAPH**, the latter using **WHIZARD** for the phase-space integration has been presented in [4]. In addition, results achieved by different generators for selected top quark pair production channels in the massless fermion approximation can be found in [17].

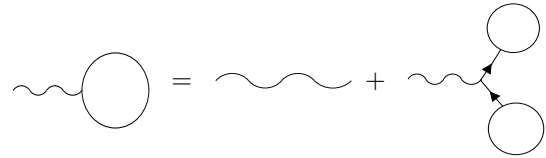
The paper is organized as follows. In Sect. 2 and 3 the relevant features of the two programs, **HELAC/PHEGAS** and **AMEGIC++**, are briefly reviewed. In Sect. 4 the results are presented and discussed. Conclusions are drawn in Sect. 5.

2 The HELAC/PHEGAS package

2.1 Amplitude Computation: HELAC

The traditional representation of the scattering amplitude in terms of Feynman graphs results in a computational cost that grows like the number of those graphs, therefore as $n!$, where n is the number of particles involved in the scattering process.

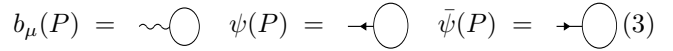
An alternative to the Feynman graph representation is provided by the Dyson-Schwinger approach. Dyson-Schwinger equations recursively express the n -point Green's functions in terms of the 1-, 2-, ..., $(n-1)$ -point functions. For instance in QED these equations can be written as follows:



$$\text{wavy line with circle} = \text{wavy line} + \text{wavy line with two circles} \quad (1)$$

$$b^\mu(P) = \sum_{i=1}^n \delta_{P=p_i} b^\mu(p_i) + \sum_{P=P_1+P_2} (ig) \Pi_\nu^\mu \bar{\psi}(P_2) \gamma^\nu \psi(P_1) \epsilon(P_1, P_2) \quad (2)$$

where



$$b_\mu(P) = \text{wavy line with circle} \quad \psi(P) = \text{fermion line with incoming arrow and circle} \quad \bar{\psi}(P) = \text{fermion line with outgoing arrow and circle} \quad (3)$$

describes a generic n -point Green function with one outgoing photon, fermion or antifermion leg, respectively, carrying momentum P . $\Pi_{\mu\nu}$ stands for the boson propagator and ϵ takes into account the sign due to fermion anti-symmetrization.

Technical details about the implementation of the algorithm for the electroweak interactions can be found in [1]. For QCD amplitudes, colour representation and summation play an important role. Usually, for the n -gluon amplitude the well known colour decomposition is used

$$\mathcal{M} = 2ig^{n-2} \sum_{P(2,\dots,n)} \text{Tr}(t^{a_1} \dots t^{a_n}) \mathcal{C}(1, \dots, n) \quad (4)$$

For processes involving quarks a similar expression may be derived. For further details, the reader is referred to the vast literature on the subject [18]. Methods for calculating the C -functions have been developed [19], including some recent ones, more suitable for multiparticle processes [20, 21]. One of the most interesting aspects of this decomposition is the fact that the C -functions satisfy certain useful properties, such as gauge invariance and cyclic symmetry. Nevertheless, the computational complexity is rather high and the evaluation of the squared colour matrix a rather complicated task [22].

In **HELAC** a novel approach has been considered. It is based on the colour connection (or colour flow) representation of the interaction vertices, where the explicit reference to the

colour has been avoided, as is also the case in the usual colour decomposition. The advantage, however, is that the colour factors acquire a much simpler form, which moreover holds for gluon as well as for quark amplitudes, leading to a unified approach *for any tree-order process involving any number of coloured partons*. Moreover, the unweighting procedure is significantly facilitated, since the usual information on colour connections, needed by the parton shower Monte Carlo, is automatically available, without any further calculation. The colour factor is universally given by

$$\mathcal{F}_I = \delta_{1\sigma_I(1)} \delta_{2\sigma_I(2)} \dots \delta_{n\sigma_I(n)}, \quad (5)$$

whereas the colour matrix, defined as

$$\mathcal{M}_{IJ} = \sum_{\text{colours}} \mathcal{F}_I \mathcal{F}_J^\dagger \quad (6)$$

with the summation running over all colours, $1 \dots N_c$, has a very simple representation:

$$\mathcal{M}_{IJ} = N_c^{m(\sigma_I, \sigma_J)}. \quad (7)$$

Here, $1 \leq m(\sigma_I, \sigma_J) \leq n$ counts the number of cycles made by the elements of the permutations σ_I and σ_J . Details can be found in ref. [23].

2.2 Phase-space integration: PHEGAS

The study of multiparticle processes, such as six-fermion production in e^+e^- , requires efficient phase-space Monte Carlo generators. The reason is that the squared amplitude, being a complicated function of the kinematical variables, exhibits strong variations in specific regions and/or directions of the phase space, lowering in a substantial way the speed and the efficiency of the Monte Carlo integration. A well known way out of this problem relies on algorithms characterized by two main ingredients:

1. The construction of appropriate mappings of the phase space parametrization, in such a way that the main variation of the integrand can be described by a set of almost uncorrelated variables, and
2. A self-adaptation procedure that reshapes the generated phase-space density in order to be as close as possible to the integrand.

In order to construct appropriate mappings, it is important to note that the integrand, i.e. the squared amplitude, has a well-defined representation in terms of Feynman diagrams. It is therefore natural to associate to each Feynman diagram a phase-space mapping that parametrizes the leading variation coming from it. In **PHEGAS**, information from **HELAC** is used to automatically construct a representation of all Feynman graphs contributing to the given process. The subset of Feynman graphs that results in a different phase-space parametrization is then used as kinematical mappings, called channels, to perform the Monte Carlo integration. Details can be found in [2].

Since in six- and eight-fermion production a large number of kinematical channels contribute, typically of the order of 10^2 to 10^4 , the optimization is also used to reduce their number. This is based on the fact that many of the channels exhibit an important correlation that renders them practically useless as separate channels. The reduction in the number of channels achieved by this optimization is generally important, resulting in a very efficient and rapid integration.

The main points can be summarized as follows:

- The algorithm exhibits a computational cost that grows like $\sim 3^n$, in contrast to the $n!$ growth of the Feynman graph approach. Therefore there is no severe limitation in computing many-particle amplitudes (up to at least 12 external).
- All electroweak vertices in both the Feynman and the Unitary gauge have been included, allowing highly non-trivial checks to be performed. The QCD interactions have been implemented in the colour-connection representation, allowing also a fast unweighting procedure. The decay width of unstable particles is introduced in the fixed-width and complex-mass schemes. Any process with any type of Standard Model particle can be reliably computed.
- Special features include also the possibility to use higher precision floating point arithmetic, allowing full control over all possible phase-space regions. Speeding up techniques, for helicity Monte Carlo treatment and large N_c estimates, are also available.
- Incorporation of higher order corrections (currently available Fermion-Loop corrections up to three-point functions) and the introduction of the Minimal Supersymmetric Standard Model are in progress.

3 The program AMEGIC++

AMEGIC++, acronym for (A Matrix Element Generator in C++), is a multi-purpose parton-level generator written in C++. It provides a convenient tool for the calculation of cross sections for scattering processes at the tree level in the framework of the SM and the MSSM. Recently the code was extended to cover processes in the ADD model of large extra dimensions as well [24]. The program can also be used to generate single events and it is one of the modules for the new complete event simulation framework **SHERPA** [25]. As such, the single events of **AMEGIC++** can be handed over to the parton shower module **APACIC++** [26] with the help of a new method that is correct at the next-to-leading logarithmic accuracy [27] and are thus linked correctly to fragmentation.

In **AMEGIC++**, full sets of Feynman diagrams are constructed automatically and are translated by the program into helicity amplitudes in a formalism similar to the one in [28]. The colour structure of each diagram is represented as a word string, the emerging structures are grouped into sets of amplitudes with identical, common colour structure. Based on them, a matrix of colour factors between amplitudes is calculated using the ordinary $SU(3)$ algebra. A number of refinements of the helicity method has

been implemented within the code as well. First of all, the algorithm presented in [29] fixes the relative signs of amplitudes when Majorana fermions are present. Furthermore, explicit polarizations for massive or massless external spin-1 bosons are enabled, allowing us to consider polarized cross sections. Similar considerations help to replace numerators of spin-1 propagators by summing over suitably defined polarizations for off-shell particles disentangling nested Lorentz structures emerging for amplitudes with many internal spin-1 bosons. As a result, **AMEGIC++** needs only quite a limited set of building blocks to construct all helicity amplitudes. Internally, they are represented as word strings employing some knowledge-storing mechanism that ensures that all building blocks have to be evaluated only once for each call of the full matrix element. With the help of internal methods these word strings are further simplified. Furthermore, another massive gain in efficiency has been achieved by summing amplitudes with identical colour structure and by algorithms for finding common factors. This is exemplified in Fig. 1. Having performed these manipulations, the resulting helicity amplitudes are stored in library files.

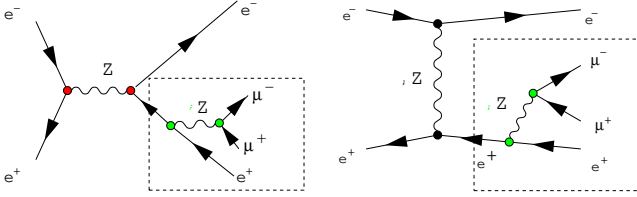


Fig. 1. Factoring out common pieces of amplitudes with identical colour structure. In the example above, the parts within the boxes are identical, hence the two amplitudes can be added and the terms inside the box can be factored out.

There are a number of prescriptions to treat unstable particles. At the moment, **AMEGIC++** supports the fixed-width scheme (FWS) and the complex-mass scheme (CMS). Defining the complex mass parameters of the electroweak gauge bosons, the Higgs boson and the top quark in terms of the real masses and the constant widths through

$$\begin{aligned} M_V^2 &= m_V^2 - i\Gamma_V m_V, \quad V = W, Z \\ M_H^2 &= m_H^2 - i\Gamma_H m_H, \quad M_t = m_t - i\Gamma_t/2, \end{aligned} \quad (8)$$

the corresponding propagators can be written as

$$\begin{aligned} D_F^{\mu\nu}(q) &= \frac{-g^{\mu\nu} + q^\mu q^\nu / M_V^2}{q^2 - M_V^2}, \quad D_F(q) = \frac{1}{q^2 - M_H^2}, \\ S_F(q) &= \frac{\not{q} + M_t}{q^2 - M_t^2}. \end{aligned} \quad (9)$$

In the FWS, the electroweak mixing angle is defined according to

$$\sin^2 \theta_W = 1 - \frac{m_W^2}{m_Z^2}. \quad (10)$$

It is kept real. For the case of the gauge-invariant CMS, the real gauge-boson masses have to be replaced by their

complex counterparts and this parameter is therefore complex as well.

Within **AMEGIC++** the Yukawa couplings of fermions to the Higgs boson and their kinematical masses are decoupled. This allows us to study, for example, the production of Higgs bosons and their decay into b -quarks, even in those cases where the user prefers to neglect the influence of the b -mass on both the phase space and the helicity structure. For the integration over the phase space of the outgoing particles, **AMEGIC++** employs an adaptive multichannel method [6]. Similar to their implementation, generic elements for phase-space mappings such as propagator-like structures are provided. The individual Feynman diagrams are analyzed individually and one or more suitable phase-space parametrizations for each diagram are automatically created and stored in library files. As an example, consider Fig. 2, which exhibits a diagram and its translation into propagator- and decay-parametrizations. These files, both for the amplitudes and the phase-space parametrizations, are compiled and linked to the code before the actual integration starts.

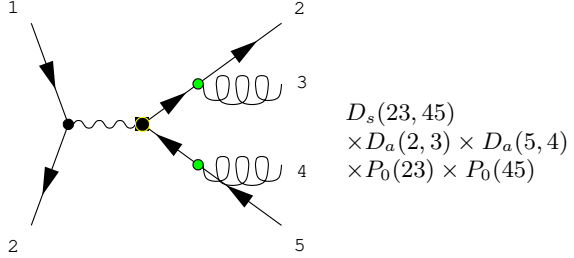


Fig. 2. Translation of a Feynman diagram into a phase-space parametrization. $D_{s,a}$ denote symmetric or asymmetric decays; the latter ones reproduce the typical feature of collinear emission of particles notorious for gauge theories with massless spin-1 bosons. The propagator terms for massless particles P_0 peak at the minimal allowed invariant mass.

For users of **AMEGIC++** only very little intervention is needed. Having specified the process(es), the model framework and its parameters, a first “initialization” run of the code results in the creation of library files. After their compilation, a second, “production” run will generate the results without any further manipulation.

4 Numerical results

4.1 Input parameters and phase-space cuts

The SM parameters are given in the G_μ scheme:

$$\begin{aligned} m_W &= 80.419 \text{ GeV}, \quad \Gamma_W = 2.12 \text{ GeV}, \\ m_Z &= 91.1882 \text{ GeV}, \quad \Gamma_Z = 2.4952 \text{ GeV}, \\ G_\mu &= 1.16639 \times 10^{-5} \text{ GeV}^{-2}, \\ \sin^2 \theta_W &= 1 - m_W^2/m_Z^2, \\ \alpha_s &= 0.0925(0.0891) \text{ at } 360(500) \text{ GeV}. \end{aligned} \quad (11)$$

The electromagnetic coupling is derived from the Fermi constant G_μ according to

$$\alpha_{\text{em}} = \frac{\sqrt{2} G_\mu M_W^2 \sin^2 \theta_W}{\pi}. \quad (12)$$

The mass of the Higgs boson is assumed to be $M_H = 130$ GeV and its associated SM tree-level width is $\Gamma_H = 0.00429$ GeV. For this Higgs boson mass its branching ratios $H \rightarrow b\bar{b}$ and $H \rightarrow W^+ W^- \rightarrow 4f$ are of the same order and therefore both decay channels signify its occurrence as an intermediate state. For the massive fermions, the following masses have been used:

$$\begin{aligned} m_\mu &= 105.6583 \text{ MeV}, & m_\tau &= 1.777 \text{ GeV}, \\ m_u &= 5 \text{ MeV}, & m_d &= 10 \text{ MeV}, \\ m_s &= 200 \text{ MeV}, & m_c &= 1.3 \text{ GeV}, \\ m_b &= 4.8 \text{ GeV}, \\ m_t &= 174.3 \text{ GeV}, & \Gamma_t &= 1.6 \text{ GeV}. \end{aligned} \quad (13)$$

The constant widths of the electroweak gauge bosons, the Higgs boson and the top quark are introduced via the fixed-width scheme as defined in Sect. 3. CKM mixing of the quark generations and the coupling of the Higgs boson to the very light fermion flavors (e , u , d) is neglected.

Concerning the phase-space integration, the following cuts are applied on the external particles:

$$\begin{aligned} \theta(l, \text{beam}) &> 5^\circ, & \theta(l, l') &> 5^\circ, & E_l &> 10 \text{ GeV}, \\ \theta(q, \text{beam}) &> 5^\circ, & \theta(l, q) &> 5^\circ, & E_q &> 10 \text{ GeV}, \\ m(q, q') &> 10 \text{ GeV}, \end{aligned} \quad (14)$$

where $\theta(i, j)$ specifies the angle between the particles i and j in the center-of-mass frame, and l , q and beam denote charged leptons, quarks or gluons and the beam electrons or positrons, respectively. The invariant mass of a jet pair qq' is denoted by $m(q, q')$.

All results presented here are obtained using 10^6 points (before cuts); statistical errors of the Monte Carlo integrations, i.e. one standard deviation, are given in parentheses.

4.2 Results

First of all, processes have been considered that serve as signals or backgrounds for the production and decay of top pairs, Table 1. Since the branching ratio is practically 100% for the decay of top quarks into bottom quarks and a W ($t \rightarrow bW^+$, $\bar{t} \rightarrow \bar{b}W^-$), all modes considered include a pair of bottom quarks. In cases involving a mixture of top production and decay and pure QCD diagrams, the relative importance of the different contributions to the total cross section has been estimated by switching on and off the QCD coupling constant. In both cases (the fully hadronic mode $b\bar{b}u\bar{u}d\bar{d}$ and the semileptonic mode $b\bar{b}u\bar{d}e^-\bar{\nu}_e$) the top contribution is by far the dominating channel; the difference of taking into account the QCD contributions or neglecting them is of the order of 2-3%.

Final state	Top-quark channels		
	QCD	AMEGIC++ [fb]	HELAC [fb]
$b\bar{b}u\bar{d}d\bar{u}$	yes	32.90(15)	33.05(14)
	yes	49.74(21)	50.20(13)
	no	32.22(34)	32.12(19)
	no	49.42(44)	50.55(26)
$b\bar{b}u\bar{u}gg$	–	11.23(10)	11.136(41)
	–	9.11(13)	8.832(43)
$b\bar{b}gggg$	–	18.82(13)	18.79(11)
	–	24.09(18)	23.80(17)
$b\bar{b}u\bar{d}e^-\bar{\nu}_e$	yes	11.460(36)	11.488(15)
	yes	17.486(66)	17.492(41)
	no	11.312(37)	11.394(18)
	no	17.366(68)	17.353(31)
$b\bar{b}e^+\nu_e e^-\bar{\nu}_e$	–	3.902(31)	3.885(7)
	–	5.954(55)	5.963(11)
$b\bar{b}e^+\nu_e \mu^-\bar{\nu}_\mu$	–	3.847(15)	3.848(7)
	–	5.865(24)	5.868(10)
$b\bar{b}\mu^+\nu_\mu \mu^-\bar{\nu}_\mu$	–	3.808(16)	3.861(19)
	–	5.840(30)	5.839(12)

Table 1. The cross sections for possible signals and backgrounds of top quark pair production in e^+e^- annihilation. All results in fb for $\sqrt{s} = 360$ GeV (first row) and $\sqrt{s} = 500$ GeV (second row).

Also, the total cross section of the fully hadronic channel is substantially larger than the cross section of any other individual $b\bar{b}+4$ jets mode.

For the QCD contributions, a similar pattern arises also in the vector-boson fusion channels, cf. Tables 2 and 3. These channels are characterized by either an electron-positron or an electron-neutrino anti-neutrino pair in the final state, corresponding to either Z boson or to W boson fusion processes, respectively. Again, switching on and off the QCD coupling constant gives rise to differences on the level of a few per cent. In contrast, taking into account the Higgs boson (Table 2) which may be produced in the s -channel through the fusion of two t -channel vector bosons, or neglecting it (Table 3) changes the total cross sections for all channels considered by a factor of 2 or larger. This is especially pronounced for channels that can be identified as WW -fusion channels with a semileptonic or fully hadronic decay of the W -pair produced by the Higgs decay (i.e. $\nu_e \bar{\nu}_e u\bar{d}e^-\bar{\nu}_e$ and $\nu_e \bar{\nu}_e u\bar{d}\mu^-\bar{\nu}_\mu$, or $\nu_e \bar{\nu}_e u\bar{d}d\bar{u}$, respectively), where the cross sections are larger by one order of magnitude.

Another mode for Higgs production at an electron-positron collider is Higgs-strahlung, where the Higgs boson is radiated off a Z -boson in the s -channel. In Table 4, total cross sections for such modes are displayed, where the Z boson decays into muons and the Higgs boson goes into four fermions through a pair of W or Z bosons. In Table 5, identical total cross sections for the same final states, but neglecting the Higgs contribution, are shown. In both cases, again, the size of the pure QCD contributions is found to be small for most final states, i.e. of the order of few per cent. The only exception is for a

Vector fusion with Higgs exchange			
Final state	QCD	AMEGIC++ [fb]	HELAC [fb]
$e^-e^+u\bar{u}d\bar{d}$	yes	0.6842(85)	0.6858(31)
	yes	1.237(15)	1.265(5)
	no	0.6453(62)	0.6527(35)
	no	1.206(14)	1.2394(75)
$e^-e^+u\bar{u}e^-e^+$	–	6.06(36)e-03	6.113(87)e-03
	–	6.58(23)e-03	6.614(80)e-03
$e^-e^+u\bar{u}\mu^-\mu^+$	–	9.24(12)e-03	9.04(11)e-03
	–	9.25(17)e-03	9.145(74)e-03
$\nu_e\bar{\nu}_eu\bar{d}d\bar{u}$	yes	1.15(3)	1.176(6)
	yes	2.36(7)	2.432(12)
	no	1.14(3)	1.134(5)
	no	2.35(7)	2.429(13)
$\nu_e\bar{\nu}_eu\bar{d}e^-\bar{\nu}_e$	–	0.426(11)	0.4309(48)
	–	0.916(30)	0.9121(48)
$\nu_e\bar{\nu}_eu\bar{d}\mu^-\bar{\nu}_\mu$	–	0.425(12)	0.4221(30)
	–	0.878(27)	0.8888(47)

Table 2. The cross sections for different $e^+e^- \rightarrow 6f$ final states corresponding to the Higgs production via vector-boson fusion signal. All results in fb for $\sqrt{s} = 360$ GeV (first row) and $\sqrt{s} = 500$ GeV (second row).

Vector fusion without Higgs exchange			
Final state	QCD	AMEGIC++ [fb]	HELAC [fb]
$e^-e^+u\bar{u}d\bar{d}$	yes	0.4838(50)	0.4842(25)
	yes	1.0514(97)	1.0445(51)
	no	0.4502(31)	0.4524(23)
	no	1.0239(79)	1.0227(43)
$e^-e^+u\bar{u}e^-e^+$	–	3.757(98)e-03	3.577(43)e-03
	–	4.082(56)e-03	4.214(46)e-03
$e^-e^+u\bar{u}\mu^-\mu^+$	–	5.201(61)e-03	5.119(70)e-03
	–	5.805(67)e-03	5.828(49)e-03
$\nu_e\bar{\nu}_eu\bar{d}d\bar{u}$	yes	0.15007(53)	0.15070(64)
	yes	0.4755(21)	0.4711(24)
	no	0.12828(42)	0.12793(55)
	no	0.4417(19)	0.4398(21)
$\nu_e\bar{\nu}_eu\bar{d}e^-\bar{\nu}_e$	–	0.04546(13)	0.04564(19)
	–	0.16033(63)	0.16011(78)
$\nu_e\bar{\nu}_eu\bar{d}\mu^-\bar{\nu}_\mu$	–	0.04230(12)	0.04180(16)
	–	0.14383(53)	0.14439(65)

Table 3. The backgrounds to Higgs production via vector boson fusion. All contributions from intermediate Higgs bosons are neglected. Cross sections are given in fb for $\sqrt{s} = 360$ GeV (first row) and $\sqrt{s} = 500$ GeV (second row).

pair of muons and four identical quarks; there, the inclusion of QCD changes the results by roughly 20%, when the Higgs boson is taken into account, and by a factor of roughly 2 when its contribution is neglected. It is amusing to note that this relative factor of two compares in size with the effect of including the Higgs boson itself. This, however, is true only for the mode that can be imagined as $e^+e^- \rightarrow ZH \rightarrow ZZZ \rightarrow \mu^+\mu^-u\bar{u}u\bar{u}$. In all other cases, as said before, inclusion of QCD has minor effects only; the

Higgs production through Higgs-strahlung			
Final state	QCD	AMEGIC++ [fb]	HELAC [fb]
$\mu^-\mu^+\mu^-\bar{\nu}_\mu e^-\bar{\nu}_e$	–	0.03244(27)	0.03210(15)
	–	0.03747(29)	0.03749(32)
$\mu^-\mu^+u\bar{d}e^-\bar{\nu}_e$	–	0.0924(8)	0.09306(46)
	–	0.1106(22)	0.10901(66)
$\mu^-\mu^+\mu^-\mu^+e^-e^+$	–	2.828(67)e-03	2.923(52)e-03
	–	2.731(65)e-03	2.691(42)e-03
$\mu^-\mu^+u\bar{u}d\bar{d}$	yes	0.2534(24)	0.2540(16)
	yes	0.2634(22)	0.2642(15)
	no	0.2441(23)	0.2471(15)
$\mu^-\mu^+u\bar{u}u\bar{u}$	no	0.2593(22)	0.2589(14)
	yes	1.125(8)e-02	1.135(22)e-02
	yes	8.767(65)e-03	8.978(58)e-03
	no	7.929(57)e-03	8.078(92)e-03
	no	6.098(35)e-03	6.013(26)e-03

Table 4. The cross sections for different $e^+e^- \rightarrow 6f$ final states corresponding to the Higgs-strahlung signal. All results given in fb for $\sqrt{s} = 360$ GeV (first row) and $\sqrt{s} = 500$ GeV (second row).

Backgrounds to Higgs-strahlung

Final state	QCD	AMEGIC++ [fb]	HELAC [fb]
$\mu^-\mu^+\mu^-\bar{\nu}_\mu e^-\bar{\nu}_e$	–	0.01845(14)	0.01843(13)
	–	0.03054(23)	0.03092(19)
$\mu^-\mu^+u\bar{d}e^-\bar{\nu}_e$	–	0.05284(57)	0.05209(33)
	–	0.08911(53)	0.08925(48)
$\mu^-\mu^+\mu^-\mu^+e^-e^+$	–	2.204(52)e-03	2.346(49)e-03
	–	2.280(66)e-03	2.277(62)e-03
$\mu^-\mu^+u\bar{u}d\bar{d}$	yes	0.1412(10)	0.1404(11)
	yes	0.2092(12)	0.2075(13)
	no	0.1358(20)	0.1341(12)
$\mu^-\mu^+u\bar{u}u\bar{u}$	no	0.2040(12)	0.2015(11)
	yes	5.937(24)e-03	5.937(25)e-03
	yes	6.134(29)e-03	6.108(27)e-03
	no	2.722(10)e-03	2.710(11)e-03
	no	3.290(12)e-03	3.303(12)e-03

Table 5. Background contributions to the Higgsstrahlungs signal for various $6f$ final states. All diagrams with intermediate Higgs bosons have been neglected. Cross sections are given in fb for $\sqrt{s} = 360$ GeV (first row) and $\sqrt{s} = 500$ GeV (second row).

Higgs boson in contrast roughly doubles the total cross section in all the other channels.

One of the salient research goals at a potential linear collider operating at energies around 500 GeV is the determination of the Higgs potential. For this, the self-couplings of the Higgs bosons have to be checked. In the framework of this publication, results are provided for the channel where the Higgs bosons emerge in Higgs-strahlungs-like topologies and decay into a pair of bottom quarks. This leads to final states $\mu^+\mu^- + 4b$, where the muons mainly come from the Z bosons. Results for total cross sections for the process $e^+e^- \rightarrow \mu^+\mu^- + 4b$, where contributions mediated by Higgs bosons have been included or neglected,

Triple Higgs coupling			
Final state	QCD	AMEGIC++ [fb]	HELAC [fb]
$\mu^- \mu^+ b\bar{b}b\bar{b}$	yes	2.560(26)e-02	2.583(26)e-02
	yes	3.096(60)e-02	3.019(43)e-02
	no	1.711(55)e-02	1.666(28)e-02
	no	2.34(12)e-02	2.36(10)e-02

Table 6. Cross sections for the process $e^+ e^- \rightarrow \mu^- \mu^+ b\bar{b}b\bar{b}$. All results in fb for $\sqrt{s} = 360$ GeV (first row) and $\sqrt{s} = 500$ GeV (second row).

Backgrounds to triple Higgs coupling			
Final state	QCD	AMEGIC++ [fb]	HELAC [fb]
$\mu^- \mu^+ b\bar{b}b\bar{b}$	yes	7.002(32)e-03	7.044(22)e-03
	yes	6.308(24)e-03	6.364(21)e-03
	no	2.955(11)e-03	2.972(12)e-03
	no	3.704(15)e-03	3.695(13)e-03

Table 7. Cross sections for $e^+ e^- \rightarrow \mu^- \mu^+ b\bar{b}b\bar{b}$ with all contributions due to intermediate Higgs bosons left out. All results in fb taken for $\sqrt{s} = 360$ GeV (first row) and $\sqrt{s} = 500$ GeV (second row).

are given in Tables 6 and 7, respectively. From the results displayed one can read off that the inclusion of intermediate Higgs bosons enhances the cross sections by a factor of three to four. Again, also the effect of QCD has been checked. For the process involving the intermediate Higgs bosons, QCD leads to total cross sections that are larger by roughly 30%-40%, without the Higgs bosons, QCD contributes on the level of factors of two to three.

5 Summary of results

In the framework of this comparison, total cross sections for 86 different processes involving six-particle final states have been obtained by the two multi-purpose matrix element generator packages **HELAC/PHEGAS** and **AMEGIC++**. The integration over the multidimensional phase space of the final states has been performed with Monte Carlo methods, and in all cases one million MC points have been used. For nearly all cross sections the resulting statistical error was significantly smaller than one per cent, roughly five per mille. There have been no significant differences between the two codes. To compare the results, for each process i the deviation $s^{(i)}$ of the two resulting cross sections $\sigma_H^{(i)}$ and $\sigma_A^{(i)}$ has been calculated through

$$s^{(i)} = \frac{\sigma_A^{(i)} - \sigma_H^{(i)}}{\sqrt{(\Delta\sigma_A^{(i)})^2 + (\Delta\sigma_H^{(i)})^2}}. \quad (15)$$

The distribution of the individual differences is depicted in Fig. 3. The average deviation is $\bar{s} = -0.065$, the variance in their distribution is $\sigma_s \approx 1$. The maximal difference

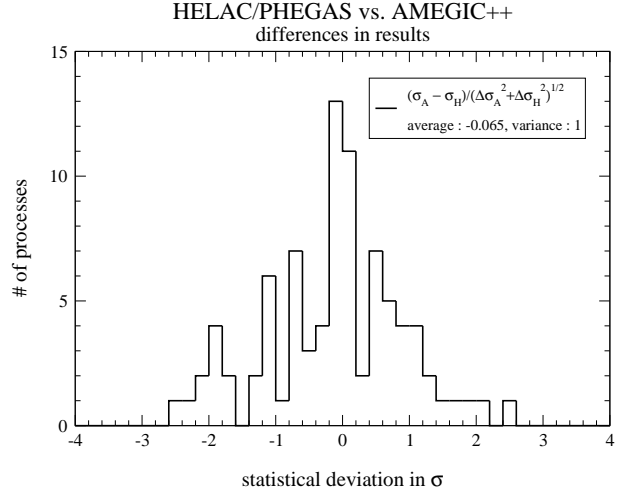


Fig. 3. The distribution of deviations $s^{(i)}$, given by Eq.15, for the eighty-six total cross sections i presented in this paper. The average value is $\bar{s} = -0.065$, their variance is $\sigma_s \approx 1$.

between two cross sections is smaller than three standard deviations, $s^{(\max.)} \approx 2.6$. The distribution of differences follows roughly a Gaussian distribution.

To summarize: Both packages, **HELAC/PHEGAS** as well as **AMEGIC++**, lead, with quite different methods, to consistent results for total cross sections for a large number of different processes with six particles in the final state. This provides an independent check of the precision level of the two codes, which can be considered as successfully tested.

Acknowledgment: The authors thank the Center for High Performance Computing Dresden (ZHR) for providing their resources and BMBF for financial support. The work of FK was supported by the EC 5th Framework Programme under contract number HPMF-CT-2002-01663. CGP also acknowledges support from the EC project "Multi-particle Processes and Higher Order Corrections", HPMF-CT-2002-01622. SS wants to thank GSI Darmstadt for financial support.

References

1. A. Kanaki and C. G. Papadopoulos, *Comput. Phys. Commun.* **132** (2000) 306 [arXiv:hep-ph/0002082].
2. C. G. Papadopoulos, *Comput. Phys. Commun.* **137** (2001) 247 [arXiv:hep-ph/0007335].
3. F. Krauss, R. Kuhn and G. Soff, *JHEP* **0202** (2002) 044 [arXiv:hep-ph/0109036].
4. S. Dittmaier and M. Roth, *Nucl. Phys. B* **642** (2002) 307 [arXiv:hep-ph/0206070].
5. K. Kolodziej, arXiv:hep-ph/0210199.
6. F. A. Berends, R. Pittau and R. Kleiss, *Nucl. Phys. B* **424** (1994) 308 [arXiv:hep-ph/9404313]; R. Kleiss and R. Pittau, *Comput. Phys. Commun.* **83** (1994) 141 [arXiv:hep-ph/9405257].
7. F. Gangemi, G. Montagna, M. Moretti, O. Nicrosini and F. Piccinini, *Eur. Phys. J. C* **9** (1999) 31 [arXiv:hep-ph/9811437]; F. Gangemi, G. Montagna, M. Moretti, O. Nicrosini and F. Piccinini, *Nucl. Phys. B* **559** (1999) 3 [arXiv:hep-ph/9905271]; F. Gangemi, arXiv:hep-ph/0002142.
8. M. Moretti, T. Ohl and J. Reuter, arXiv:hep-ph/0102195.
9. W. Kilian, LC-TOOL-2001-039.
10. T. Stelzer and W. F. Long, *Comput. Phys. Commun.* **81** (1994) 357 [arXiv:hep-ph/9401258].
11. F. Maltoni and T. Stelzer, *JHEP* **0302** (2003) 027 [arXiv:hep-ph/0208156].
12. F. Caravaglios and M. Moretti, *Phys. Lett. B* **358** (1995) 332 [arXiv:hep-ph/9507237]; *Z. Phys. C* **74** (1997) 291 [arXiv:hep-ph/9604316].
13. T. Ohl, *Comput. Phys. Commun.* **120** (1999) 13 [arXiv:hep-ph/9806432].
14. H. Murayama, I. Watanabe and K. Hagiwara, KEK-91-11.
15. M. W. Grunewald *et al.*, arXiv:hep-ph/0005309.
16. J. A. Aguilar-Saavedra *et al.*, [The ECFA/DESY LC Physics Working Group], hep-ph/0106315.
17. S. Dittmaier, [arXiv:hep-ph/0308079].
18. M. L. Mangano and S. J. Parke, “Multi-parton amplitudes in gauge theories”, *Phys. Rep.* **200**, (1991) 301-367, and references therein. [arXiv:hep-ph/9212246].
19. W.T. Giele, “Properties and calculations of multiparton processes”, PhD thesis (University of Leiden) (1989).
20. P. Draggiotis, R. H. P. Kleiss and C. G. Papadopoulos, *Phys. Lett. B* **439** (1998) 157 [arXiv:hep-ph/9807207]; P. D. Draggiotis, R. H. P. Kleiss and C. G. Papadopoulos, *Eur. Phys. J. C* **24** (2002) 447 [arXiv:hep-ph/0202201].
21. F. Caravaglios, M. L. Mangano, M. Moretti and R. Pittau, “A new approach to multi-jet calculations in hadron collisions,” *Nucl. Phys.* **B539** (1999) 215 [hep-ph/9807570]; M. L. Mangano, M. Moretti, F. Piccinini, R. Pittau and A. D. Polosa, *JHEP* **0307** (2003) 001 [arXiv:hep-ph/0206293].
22. J.G.M. Kuijf, “Multiparton production at hadron colliders”, PhD thesis (University of Leiden) (1991)
23. “HELAC-PHEGAS: automatic computation of helicity amplitudes and cross sections” by A. Kanaki and C. G. Papadopoulos, Second CPP Symposium-Computational Particle Physics, KEK Proceedings 2002-11, Editor: Y. Kurihara, August 2002, pp. 20-25.
24. T. Gleisberg, F. Krauss, K. T. Matchev, A. Schälicke, S. Schumann and G. Soff, *JHEP* **0309** (2003) 001 [arXiv:hep-ph/0306182].
25. T. Gleisberg, S. Höche, F. Krauss, A. Schälicke, S. Schumann and J. Winter, CERN-TH/2003-284 and hep-ph/0311263.
26. R. Kuhn, F. Krauss, B. Ivanyi and G. Soff, *Comput. Phys. Commun.* **134** (2001) 223 [arXiv:hep-ph/0004270].
27. S. Catani, F. Krauss, R. Kuhn and B. R. Webber, *JHEP* **0111** (2001) 063 [arXiv:hep-ph/0109231]; F. Krauss, *JHEP* **0208** (2002) 015 [arXiv:hep-ph/0205283].
28. R. Kleiss and W. J. Stirling, *Nucl. Phys. B* **262** (1985) 235; A. Ballestrero, E. Maina and S. Moretti, *Nucl. Phys. B* **415** (1994) 265
29. A. Denner, H. Eck, O. Hahn and J. Kublbeck, *Nucl. Phys. B* **387** (1992) 467.